UNIVERSITY OF LEEDS

This is a repository copy of *Uptake of acetylene on cosmic dust and production of benzene in Titan's atmosphere*.

Uptake of Acetylene on Cosmic Dust and Production of Benzene in Titan's Atmosphere

Victoria L. Frankland[1], Alexander D. James[1], Juan Diego Carrillo Sánchez[1], Thomas P. Mangan[1], Karen Willacy[2], Andrew R. Poppe[3] and John M. C. Plane[1]*

1. School of Chemistry, University of Leeds, Leeds, LS2 9JT, UK

2. Jet Propulsion Laboratory, California Institute of Technology, CA 91109, USA

3. Space Sciences Laboratory, University of California at Berkeley, Berkeley, CA 94720, USA

* Corresponding author: j.m.c.plane@leeds.ac.uk, +44 113 3438044

Abstract

A low-temperature flow tube and ultra-high vacuum apparatus were used to explore the uptake and heterogeneous chemistry of acetylene (C_2H_2) on cosmic dust analogues over the temperature range encountered in Titan's atmosphere below 600 km. The uptake coefficient, γ, was measured at 181 K to be $(1.6 \pm 0.4) \times 10^{-4}$, $(1.9 \pm 0.4) \times 10^{-4}$ and $(1.5 \pm 0.4) \times 10^{-4}$ for the uptake of C_2H_2 on Mg_2SiO_4, $MgFeSiO_4$ and Fe_2SiO_4, respectively, indicating that γ is independent of Mg or Fe active sites. The uptake of C_2H_2 was also measured on SiO_2 and SiC as analogues for meteoric smoke particles in Titan's atmosphere, but was found to be below the detection limit ($\gamma < 6 \times 10^{-8}$ and $< 4 \times 10^{-7}$, respectively). The rate of cyclo-trimerization of C_2H_2 to C_6H_6 was found to be $2.6 \times 10^{-5} \exp(-741/T)$ s^{-1}, with an uncertainty ranging from $\pm$ 27 % at 115 K to $\pm$ 49 % at 181 K. A chemical ablation model was used to show that the bulk of cosmic dust particles (radius 0.02 - 10 μm) entering Titan's atmosphere do not ablate (< 1% mass loss through sputtering), thereby providing a significant surface for heterogeneous

chemistry. A 1D model of dust sedimentation shows that the production of C_6H_6 *via* uptake of C_2H_2 on cosmic dust, followed by cyclo-trimerization and desorption, is probably competitive with gas-phase production of C_6H_6 between 80 and 120 km.

Keywords: Titan Atmosphere; Cyclo-trimerization of acetylene; Benzene formation; Cosmic dust; Kuiper belt.

1. Introduction

Titan, the largest moon of Saturn, is the only moon in the Solar System to have a significant atmosphere. In the lower atmosphere, a thick haze is observed (Rages and Pollack, 1983; Smith et al., 1981) with the main haze region occurring from ~ 220 km to the surface. A detached haze layer lies in the mesopause region around 500 km (Liang et al., 2007; Porco et al., 2005; Shemansky et al., 2005). The processes which drive formation of these haze layers are still unclear but are considered to be linked to the formation of organic aerosols (tholins). Simple organic species, such as acetylene (C_2H_2), ethylene (C_2H_4), ethane (C_2H_6), benzene (C_6H_6) and hydrogen cyanide (HCN), provide feedstocks for formation of these aerosols (Flasar et al., 2005; Shemansky et al., 2005; Waite et al., 2005).

C_2H_2 is the second most abundant minor species after C_2H_6 (Vinatier et al., 2010) and is predominantly formed by photodissociation of C_2H_4 above ~600 km (Krasnopolsky, 2014). The vertical profile of C_2H_2 was determined by Teanby et al. (2006), who obtained a mixing ratio of 4×10^{-6} between 230 and 500 km.

Photochemical models of Titan's atmosphere have been constructed based on observational data and extrapolating the rate coefficients of pertinent chemical reactions to low temperatures (Coustenis et al., 2010; Dobrijevic et al., 2014; Hebrard et al., 2007; Hebrard et al., 2013; Krasnopolsky, 2010; Krasnopolsky, 2012; Krasnopolsky, 2014; Lara et al., 2014;

Lavvas et al., 2008a; Lavvas et al., 2008b; Magee et al., 2009; Wilson and Atreya, 2003; Wilson and Atreya, 2004; Wilson et al., 2003). These models, based on kinetics measured in the laboratory, reveal that the major loss pathways for C_2H_2 are: hydrogenation to C_2H_4; formation of C_4H_2 (which can go on to form more complex hydrocarbons); and condensation out of the gas phase near ~ 80 km (Vinatier et al., 2010). However, none of these models have considered adsorption and heterogeneous chemistry on cosmic dust or meteoric smoke particles (MSPs); the latter form from the recondensation of metallic vapours produced by meteoric ablation (Saunders and Plane, 2011).

Contributions to the flux of cosmic dust entering Titan's atmosphere are thought to originate from several sources including Edgeworth-Kuiper Belt (EKB) objects and various cometary families (e.g., Jupiter family and Halley type comets) (Landgraf et al., 2002; Poppe, 2016; Poppe and Horanyi, 2012). Dust from EKB objects forms through either mutual collisions or interstellar dust bombardment (Stern, 1996; Yamamoto and Mukai, 1998), while cometary grains originate from sublimation and/or sporadic outbursts (e.g., Sekanina (1996); Kelley et al. (2013)). Data collected from the Pioneer 10 meteoroid detector and from the Student Dust Counter (SDC) on the New Horizons mission has been used to constrain the overall mass production rate from the EKB and the differential mass production distribution into the Saturnian system, including Saturn's satellites and planetary rings (Han et al., 2011; Poppe and Horanyi, 2012). Investigations of cometary dust (e.g. Zolensky et al. (2006) and Gainsforth et al. (2015)) assume the cosmic dust to have the composition of carbonaceous chondrites which, in this study, are represented by olivines ($Mg_{2-2n}Fe_{2n}SiO_4$ where $0 \leq n \leq 1$).

Only a small fraction of the cosmic dust entering Titan's atmosphere will actually ablate (see Section 4.1). Ablation occurs between 450 – 700 km, giving rise to layers of metal atoms such

as Na, Fe, Mg and Si (English et al., 1996; Ip, 1990; Molina-Cuberos et al., 2008). These atoms may react with various unsaturated hydrocarbons (by addition rather than abstraction), and the metal-containing organics and nitrogen-organics then condense to form MSPs. In contrast, in the Earth's mesosphere reactions with O_3 and O_2 should lead to the formation of metal oxide and silicate MSPs (Plane et al., 2015). Both MSPs and un-ablated cosmic dust particles have the potential to interact with gas-phase species and tholins as they fall through Titan's atmosphere.

Laboratory studies have formed tholins in a N_2/CH_4 gas mixture by electron discharge and photochemistry (Cable et al., 2012; Coll et al., 2013). A range of nitrogen-rich organics and hydrocarbons are present in the tholin-like material, suggesting that co-polymerization or incorporation of small precursors (such as C_2H_2) is occurring. As the formation mechanism of tholins in Titan's atmosphere is unclear, uptake of small precursors onto MSPs and cosmic dust particles could seed the formation and the growth of tholins. If this is the case, heterogeneous chemistry on MSPs and cosmic dust particles could be a possible source for more complex organic species such as C_6H_6. This in turn could lead to further reactions resulting in the formation of poly-aromatic hydrocarbons (PAHs). Thus, greater understanding of the uptake of small precursor species and their surface chemistry on cosmic dust and MSPs is required.

One potential heterogeneous product formed from adsorbed C_2H_2 molecules on cosmic dust is C_6H_6. This conversion mechanism (known as cyclo-trimerization) has mostly been explored on pure and mixed Pd catalysts (e.g. Jungwirthova and Kesmodel (2000) and Ramirez-Cuesta et al. (1995)). In this case, cyclo-trimerization seems to occur through the rapid formation of the C_4H_4 metallocyclic intermediate species (Ormerod et al., 1993a; Pacchioni and Lambert,

4

1994; Ramirez-Cuesta et al., 1995). This species can then react with another adsorbed C_2H_2 species to form C_6H_6 (Hoffmann et al., 1992; Janssens et al., 1998; Ormerod et al., 1991; Patterson and Lambert, 1988; Patterson et al., 1989) or 2 C_4H_4 molecules react together to form cyclo-octatetraene (C_8H_8) which then thermally decomposes to yield C_6H_6 and C_2H_2 (Pacchioni and Lambert, 1994; Ramirez-Cuesta et al., 1995). Interestingly, cyclo-trimerization of C_2H_2 does not occur on MgO (Abbet et al., 2001), which is a substrate perhaps more relevant to cosmic dust analogues.

In this study, the uptake of C_2H_2 is explored on a range of cosmic dust and MSP analogues. The apparatus and experimental procedures are outlined in Section 2, and the results are discussed in Section 3. The observation of C_6H_6 formation through cyclo-trimerization of C_2H_2 on the cosmic dust analogues is also described in Section 3. Section 4 discusses the atmospheric implications for Titan's atmosphere: the estimated available surface area of sedimenting cosmic dust particles is used in a 1-D atmospheric model to compute the heterogeneous C_6H_6 formation rate through C_2H_2 uptake on cosmic dust particles, and compared with the gas-phase C_6H_6 formation rates simulated by the Caltech/JPL 1D model of Titan (Allen et al., 1981; Gladstone et al., 1996; Li et al., 2014; Yung et al., 1984; Zhang et al., 2010).

2. Experimental Procedure

2.1. Dual Flow Tube Apparatus

C_2H_2 uptake experiments were performed using a dual borosilicate (SiO_2) flow tube system (Figure 1). One flow tube contained the cosmic dust/MSP analogue sample and the other acted as a reference tube. Both tubes have an inner diameter of 1.0 cm and a length of 50

cm. The middle sections of both tubes pass through a box containing dry ice (38 cm in length). The flow tubes were connected together by a stainless steel and glass gas-handling line fitted with 3-way taps. A C_2H_2/He gas mixture and a pure He gas were admitted to only one flow tube at any one time, with the gas flows controlled by a calibrated mass flow controller (MKS Instruments, 20 sccm) and a needle valve, respectively. The pressure was measured with a gauge (MKS Baratron, 0-10 Torr) downstream of the mass flow controller. The temperatures inside both flow tubes were monitored using a K-type thermocouple. The exit downstream of the dual flow tubes was coupled through a 0.35 mm diameter orifice to a double-differentially pumped chamber equipped with a quadrupole mass spectrometer (QMS) (VG Scientific, SXP Elite). A second pumping line between the second 3-way tap and the orifice enabled the residence time of the gaseous species in the flow tube to be varied independently of the total pressure.
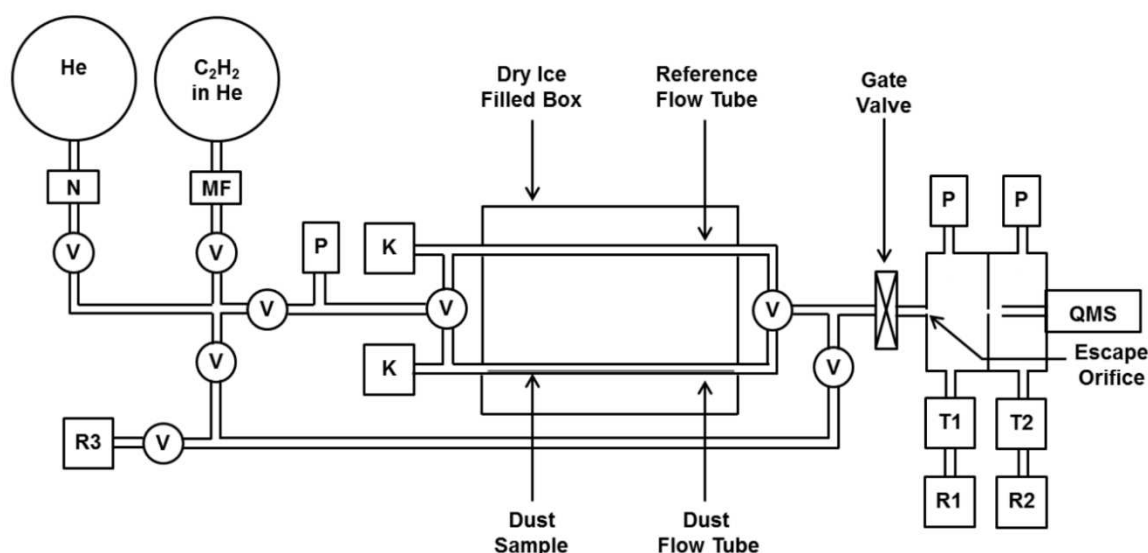
Figure 1. Schematic diagram of the dual flow tube apparatus: K = K-type thermocouples; MF = mass flow controller; N = needle valve; P = pressure gauge; QMS = quadrupole mass spectrometer; R = rotary pump T = turbo pump; V = 2- or 3-way valve.

The olivine ($MgFeSiO_4$), forsterite (Mg_2SiO_4) and fayalite (Fe_2SiO_4) cosmic dust analogues were prepared by a sol-gel process: stoichiometric amounts of magnesium chloride (Aldrich), ferrous (II) ammonium sulfate (Sigma-Aldrich) and sodium orthosilicate (Alfa Aesar) were mixed at room temperature and then stirred for 7 days to allow the reactions to go to completion (Frankland et al., 2015). Metal salt by-products were removed by repeated dialysis using a soxhlet apparatus with the particles held in water permeable tubing (Snakeskin 7000 MWCO). The products were then stored in a desiccator. Silicon carbide (SiC) particles (Sigma-Aldrich, 200-450 mesh) were used as an MSP analogue. For the uptake experiments, a sample mass (typically 0.5 g) was evenly distributed inside the dust flow tube before degassing by pumping overnight. Gas mixtures of C_2H_2 (BOC, > 98.5 %) in He (BOC, CP grade) with mixing ratios of 1.41×10^{-4}, 2.48×10^{-4} and 1.41×10^{-2} were prepared using standard manometric techniques.

Experiments were performed at 181 ± 2 K. Once the temperature inside both flow tubes had stabilised, the background levels (i.e. without a gas flow) of C_2H_2, butadiene (C_4H_4), C_6H_6 and C_8H_8 were monitored. In a typical experiment, the C_2H_2/He gas mixture (flow rate of 4.5 sccm) was passed through the reference flow tube until the mass traces were stable. The gas mixture was then re-directed through the dust flow tube. For the initial uptake experiments, the gas mixture was flowed over the dust until the mass signal stabilised before swapping back to the reference flow tube. For the uptake experiments which required the dust analogue to become fully saturated with C_2H_2, the gas flow was temporarily re-directed through the reference flow tube roughly every 50 scans in order to facilitate background correction. Once the end point had been reached (in either type of experiment), the C_2H_2 in

He gas flow was switched off (initial uptake experiment) or swapped to the pure He gas flow (full C_2H_2 saturation) which was then terminated once the flow tubes had reached ~ 260 K through the controlled removal of dry ice from the cooler box. The experiments were repeated at least 3 times for each analogue under a fixed set of conditions. Between each initial uptake experiment when the same dust analogue was used, the sample inside the dust flow tube was heated using a heat gun to roughly 60 ˚C for a minimum of 5 minutes to ensure all the C_2H_2 molecules had desorbed (confirmed by monitoring m/z = 26 with the QMS). For the full saturation uptake experiments, a fresh dust analogue sample was used.

The QMS data was background corrected with respect to the mass signal when no gas was flowing. To take into account any drift in the C_2H_2 mass signal intensity, the data from the reference flow tube was plotted against time and a line of best fit applied. This was then used to correct the reference C_2H_2 mass signal to a value of 1×10^5 counts (average initial m/z = 26 signal in the reference flow tube) over the full experiment. The drift in the C_2H_2 mass signal for the initial uptake was small (< 1000 counts over ~14 minutes) whereas the drift in the longer-duration full uptake experiments followed a decay curve (~100,000 counts over 100 minutes). The drift correction factor (with respect to time) derived from the reference flow tube was applied to the data from the dust flow tube for that experiment. An additional step to reduce the effect of the mass signal drift was to run the QMS (collecting background spectra) for at least 30 minutes prior to the start of an experiment. The same background and mass signal drift correction procedures were applied to any other masses of interest in the mass spectra.

2.2. UHV Apparatus

The heterogeneous chemistry of C_2H_2 on dust analogues was explored using an ultra-high vacuum (UHV) apparatus (Figure 2). This system has been described previously by Vondrak et al. (2006). Briefly, the ~25 L chamber is pumped by a 550 L s^{-1} turbo-molecular pump backed by a rotary pump, achieving a base pressure of typically $< 3 \times 10^{-9}$ mbar. The chamber is equipped with a quadrupole mass spectrometer (Hiden, HAL 3F 301 RC PIC), reflection-absorption infrared spectroscopy (RAIRS) system (Brucker, IFS 66/S), a needle valve (NUPRO, SS4BK) for gas dosing and an inert ion (Ar$^+$) sputter source which was modified to function as a leak valve for this study. A cylindrical stainless steel sample mount (12 mm diameter and 2.5 mm thickness) was coated on one side with a thin layer of Fe_2SiO_4 dust generated in a photochemical reactor (Saunders and Plane, 2011), and then mounted in the centre of the UHV chamber *via* tungsten (W) heating wires onto an oxygen-free high conductivity cold finger, which in turn was mounted onto an xyzθ manipulator (Figure 2). The sample was liquid nitrogen cooled to a base temperature of ~115 K and could be heated resistively using the W wires embedded through the sample mount. The surface temperature was monitored using a K-type thermocouple positioned in a small hole on the side of the sample mount. Prior to each experiment the sample was annealed at 600 K for 30 minutes. It should be noted that although cosmic dust from the EKB is thought to be richer in Mg than Fe (Gainsforth et al., 2015; Zolensky et al., 2006), the results obtained in this study show that C_2H_2 uptake and cyclo-trimerization of C_2H_2 to C_6H_6 is independent of Mg and Fe active sites at a mean temperature of 181 K. This was assumed to be the case at lower dust surface temperatures as well.
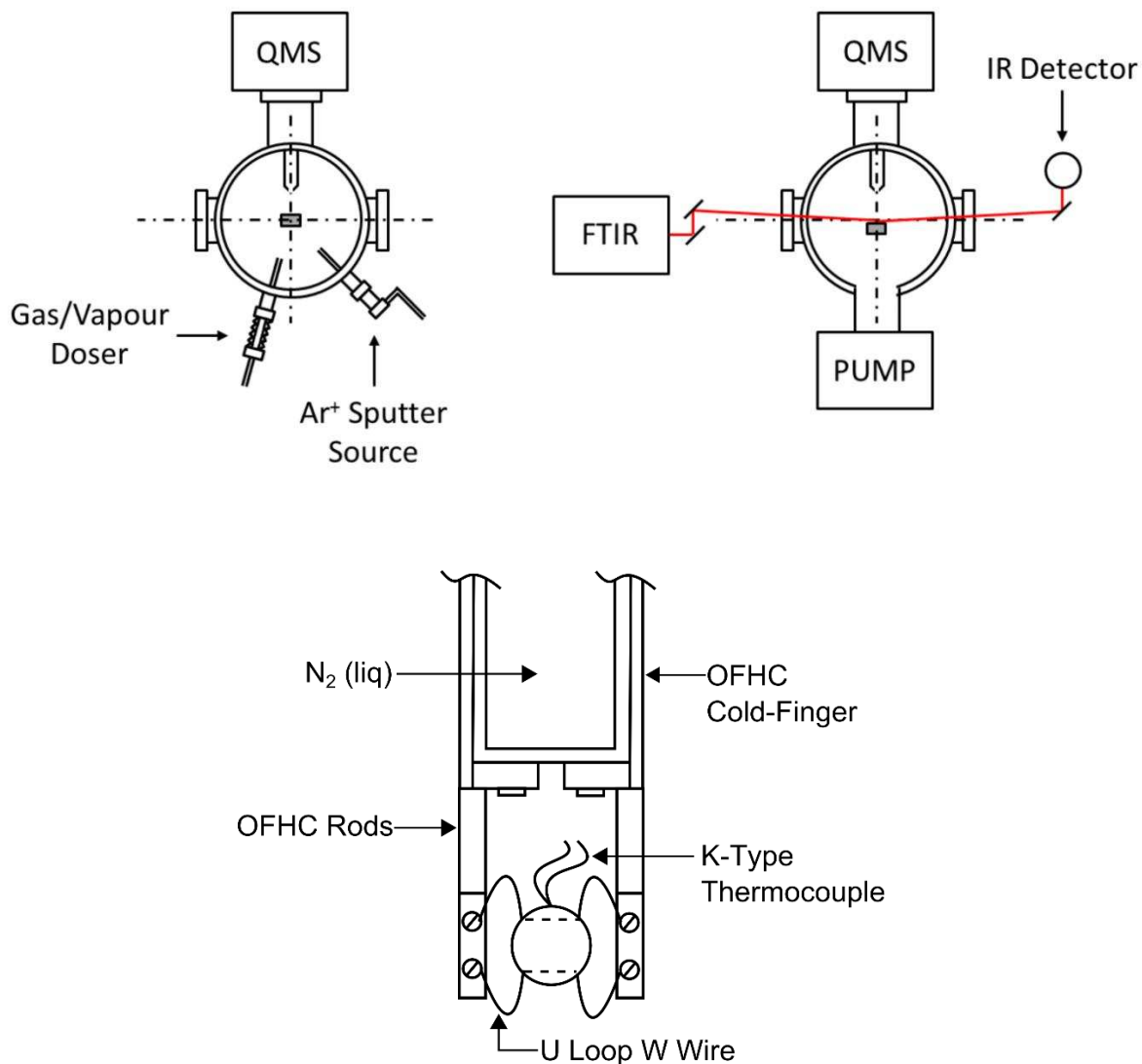
Figure 2. Schematic diagram of the upper (top left) and lower layer (top right) of the UHV apparatus, and the sample mount arrangement (bottom): QMS = quadrupole mass spectrometer (which can be situated at either layer); FTIR = Fourier transform infrared spectrometer.

C_2H_2 (BOC, > 98.5 %) was dosed onto the sample *via* the needle valve in the form of a collimated effusive beam slightly larger than the sample. This minimises adsorption (and therefore desorption) of dosed species onto other nearby surfaces such as the cold finger. Any species adsorbed onto the W wires would desorb immediately upon heating. The C_2H_2

dosing rate was calibrated using beam flux calibrations based on the procedure by Oakes (1994). Briefly, the beam flux, F_{beam}, is calculated from the exponential decay of a gas species starting from the point when the input gas flow has been terminated (Mangan et al., 2015). The exponential decay is described by:

$$P = P_0 \exp^{-C_m t} \tag{1}$$

where P is the pressure, P_0 is the initial pressure at the termination of the dose, C_m is the pumping coefficient for that gas and t is the time from the start of the decay. Equation 1 was linearised and C_m and P_0 obtained from the gradient and intercept, respectively. From this F_{beam} is given by:

$$F_{beam} = \frac{V_{system} C_m P_0}{k_B T A_{beam}} \tag{2}$$

where V_{system} is the volume of the chamber, k_B is the Boltzmann constant, T the temperature of the gaseous species and A_{beam} the cross sectional area of the molecular beam. F_{beam} in this study was $(1.3 \pm 0.1) \times 10^{14}$ molecules cm^{-2} s^{-1}.

In a typical experiment, a thin film of C_2H_2 was dosed onto the Fe_2SiO_4 sample. The sample was held at the required dosing temperature until just before the final stage of the experiment, when the sample was cooled to base temperature (115 K) before performing a temperature programmed desorption (TPD) analysis, where the sample was heated up to 600 K with a heating ramp of 0.96 ± 0.03 K s^{-1}. This ensured that all species physisorbed to the sample were desorbed, providing a clean substrate surface for the next experiment.

3. Results and Discussion

3.1. C_2H_2 Uptake Coefficient

A typical background-corrected mass spectrum for the initial uptake of C_2H_2 on Mg_2SiO_4 is displayed as a function of time in Figure 3. The plot shows a significant drop in the normalised mass spectrometer signal for C_2H_2 as the gas mixture is re-directed from the reference to the dust flow tube at ~325 s. The mass signal recovers almost instantaneously when the gas mixture is directed back to the reference flow tube at ~710 s. The rate of uptake of a gas to a solid surface is characterised by the probability that a collision will result in loss of a molecule from the gas phase. This is an empirical quantity termed the uptake coefficient, γ.
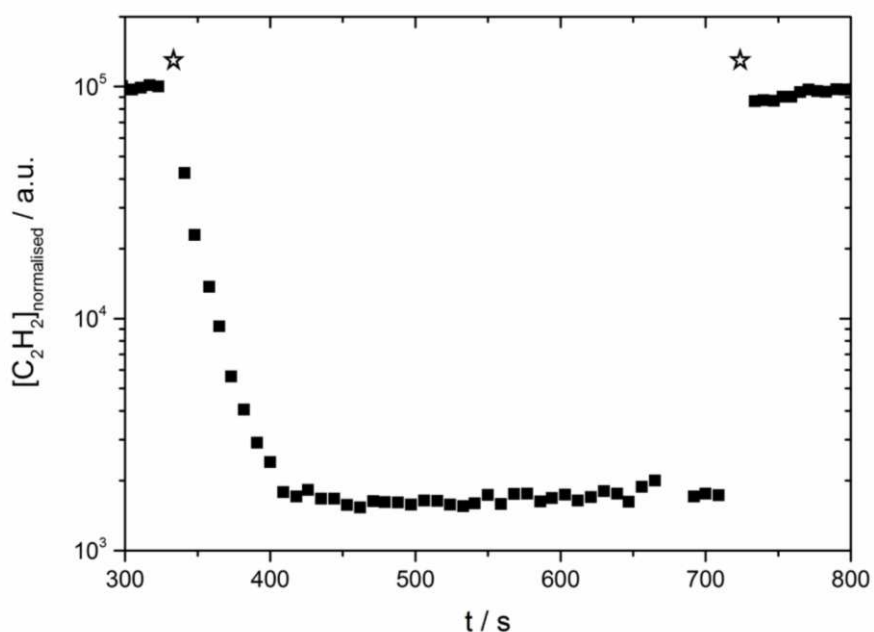
Figure 3. Typical mass spectrum of C_2H_2 uptake on forsterite. Star symbols indicate the times when the gas flow was directed from the reference to the dust and from the dust back to the reference flow tubes.

The first-order rate of loss, -d[N]/dt, of the gaseous concentration of species N is given by:

$$-\frac{d[N]}{dt} = k[N] \qquad (3)$$

where k is the rate coefficient for loss. If the residence time, τ, in the cooled section of the flow tube is significantly greater than the time for C_2H_2 molecules to diffuse to the dust surface, then the rate of loss measured at the exit from the flow tube is controlled by uptake to the surface. This condition was achieved by varying τ between 3 and 7 s, while the characteristic diffusion time across the tube was 0.01 s at a He pressure of 8 Torr. Thus k can be taken as the uptake rate coefficient, k_γ, which is calculated from:

$$k_\gamma = \frac{\gamma \bar{c} a_s}{4V} = \frac{ln([N]_0/[N]_\tau)}{\tau} \qquad (4)$$

where $\bar{c}$ is the molecular mean speed, a_s the surface area of the dust sample, V the volume of the cooled section of the flow tube, and $[N]_0$ and $[N]_\tau$ are the gas-phase concentrations of species N at the entrance and exit of the flow tube, respectively. In this study, γ was calculated by varying either a_s or τ.

One potential complication with this technique is knowledge of the fraction of the sample specific surface area which is actually involved in uptake of the gas. At one extreme, if a gas is readily taken up then it will only be the particles in the uppermost layers of the sample which will be directly involved. At the other, if γ is small then the gas will penetrate throughout the sample and be exposed to the full surface area. Possible values of a_s range from the geometric ($a_{(geo)}$, given by the cross sectional area of the dust inside the cooled region of the flow tube) to the surface area estimated from the Brunauer-Emmet-Teller (BET) isotherm ($a_{(BET)}$, determined from the uptake of N_2 gas to the surface at cryogenic temperatures)

13

(Brunauer et al., 1938). Thus, the lower limit for a_s ($a_{(GEO)}$) gives an upper limit for γ and *vice versa* for $a_s = a_{(BET)}$.

To determine the available surface area for the adsorption of C_2H_2, the uptake experiments were repeated for different sample masses. The results for Mg_2SiO_4 are displayed in Figure 4, which shows that γ remained constant (within experimental error) for the assumption that
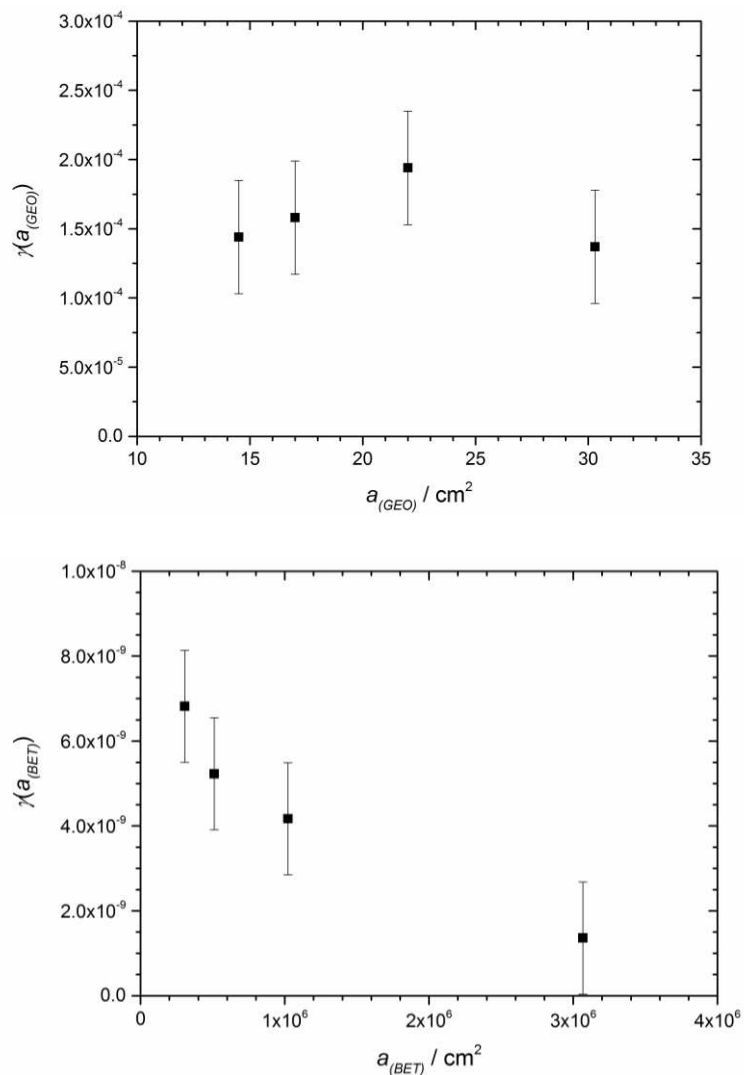
Figure 4. The uptake coefficient (γ) as a function of Mg_2SiO_4 dust surface area: upper panel, the geometric surface area ($a_{(GEO)}$); lower panel, the BET surface area ($a_{(BET)}$).

$a_s=a_{(GEO)}$. This indicates that the uptake of C_2H_2 was confined to the particles in the uppermost layers of the dust analogue. When $a_{(BET)}$ was used, the value of γ decreased with increasing mass. Since the number of active sites for sticking should increase linearly with the available surface area, less than the full BET surface area must have been available for C_2H_2 uptake in these experiments. The same behaviour was observed for Fe_2SiO_4 and $FeMgSiO_4$ (not shown). Thus, only the values of γ using $a_{(GEO)}$ as a_s for Mg_2SiO_4, $MgFeSiO_4$ and Fe_2SiO_4 are displayed in Table 1 with the error taken as 1 standard deviation of the mean between repeats.

Table 1. C_2H_2 uptake coefficients and C_2H_2-C_2H_2 average distances on the cosmic dust analogues.

| Cosmic dust analogue	γ (181 K)	C_2H_2-C_2H_2 average distance / Å
Mg_2SiO_4	$(1.6 \pm 0.4) \times 10^{-4}$	4.0 ± 0.2
$MgFeSiO_4$	$(1.9 \pm 0.4) \times 10^{-4}$	1.9 ± 0.2
Fe_2SiO_4	$(1.5 \pm 0.4) \times 10^{-4}$	2.7 ± 0.2
SiO_2	$< 5.8 \times 10^{-8}$	-
SiC	$< 3.6 \times 10^{-7}$	-

Table 1 shows that the γ values for Mg_2SiO_4, $MgFeSiO_4$ and Fe_2SiO_4 are the same within experimental error, yielding an average $\gamma = (1.7 \pm 0.4) \times 10^{-4}$. These results suggest that the uptake of C_2H_2 is independent of Mg or Fe active sites on the analogue surface, indicating that C_2H_2 uptake will occur on any un-ablated cosmic dust with an olivine (and probably pyroxene) composition. Whether the C_2H_2 uptake was controlled by SiO active sites was explored by comparing the uptake of C_2H_2 on the bare borosilicate (SiO_2) flow tube walls at 295 and 181 K. This yielded $\gamma < 5.8 \times 10^{-8}$ over this temperature range.

Uptake of C_2H_2 on SiC was also not measurable, with $\gamma < 3.6 \times 10^{-7}$ (the upper limit to γ for SiC is larger than for SiO_2 because of the difference between the geometric surface area of the

SiC analogue sample and the walls of the flow tube (14.9 and 119 cm^2, respectively)). Other MSP analogues that could be formed in Titan's atmosphere include metal-organics. However, measuring uptake on these species is not possible since they tend to be unstable in air.

Additional initial C_2H_2 uptake experiments were performed on Mg_2SiO_4 by varying τ, which was achieved by varying the mass flow rate through the flow tubes at constant, but maintaining a constant pressure by using the pumping line between the second 3-way tap and the mass spectrometer orifice (Figure 1). The average results are displayed in Figure 5 with the error taken as one standard deviation for each τ data set. A line of best fit was applied to the experimental data (solid red line) which passes through the origin (within experimental error). From the gradient, a value of $(1.9 \pm 0.4) \times 10^{-4}$ was obtained for γ, which is within experimental error of the value obtained when τ was fixed (i.e. when the value of a_s was determined).
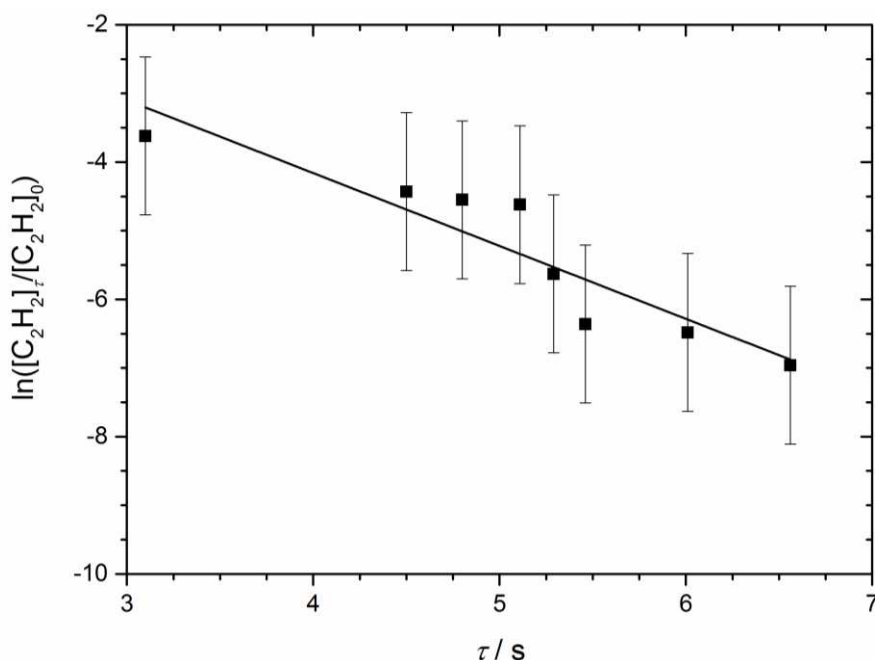
Figure 5. C_2H_2 intensity response with respect to the residence time of C_2H_2 in the flow tube, τ, on Mg_2SiO_4.

For some of the experiments on 0.5 g of Mg_2SiO_4, $MgFeSiO_4$ or Fe_2SiO_4, the uptake of C_2H_2 was continued until the C_2H_2 mass signal returned back to the pre-dust exposure level, at which point the dust analogue had become saturated. This enabled the average distance between two C_2H_2 molecules, d_{av}, to be calculated. Note that fresh dust analogue samples were used for these full saturation uptake experiments. The total number of C_2H_2 molecules adsorbed onto the C_2H_2-saturated dust in the flow tube, C_2H_{2surf}, was obtained by integrating the area above the m/z = 26 trace up to the mass signal intensity observed in the reference flow tube (after background and mass signal drift correction). d_{av} was then calculated using equation 5:

$$d_{av} = \sqrt{\frac{a_s}{C_2H_{2\,surf}}} \qquad (5)$$

where a_s was set to $a_{(GEO)}$. Table 1 shows that d_{av} ranges from 2 to 4 Å for the fully saturated Mg_2SiO_4, $MgFeSiO_4$ and Fe_2SiO_4 dust analogues. These d_{av} distances are similar to the total length of a C_2H_2 molecule (3.3 Å), which is close enough (if energy barriers are not too large) for C_2H_2 to polymerize to form products such as C_4H_4, C_6H_6 and C_8H_8.

3.2. Heterogeneous Chemistry of C_2H_2 on Olivines

The formation of C_2H_2 oligomers on Mg_2SiO_4 and Fe_2SiO_4 was explored by performing an extended version of the C_2H_2 uptake experiment (Figure 6). Once the dust analogue had become saturated (around 5650 s in Figure 6), the C_2H_2/He flow was switched to pure He and the dust temperature held at 181 K until the gas-phase C_2H_2 concentration had returned to the background level. The dust temperature was then raised through the controlled removal of dry ice from the cooler box. The resulting heating ramp is shown in the insert plot in Figure 6. The C_6H_6 mass trace was background corrected using the same procedure as for C_2H_2

(Section 2), and scaled to the C_2H_2 concentration using their respective ionization cross sections.
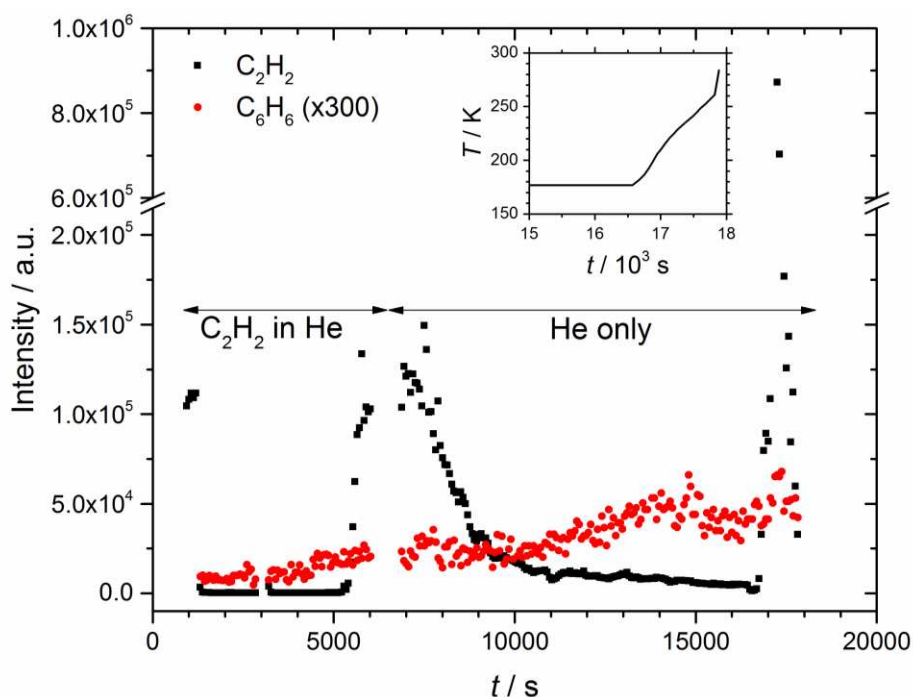
Figure 6. Uptake of C_2H_2 and conversion into C_6H_6 as a function of time. Between 1000 and 5600 s, the Fe_2SiO_4 dust analogue at 181 K became saturated when exposed to a flow of C_2H_2 in He. The flow was then switched to pure He until 16500 s, when the dust temperature was increased (temperature ramp shown in the insert plot).

During the C_2H_2 uptake part of the experiment (1000 - 5650 s in Figure 6), the gas-phase C_6H_6 signal increases, clear evidence that cyclo-trimerization of C_2H_2 is occurring on the dust surface. When the gas mixture was changed over to pure He, the intensity of C_6H_6 reached a temporary plateau for ~3500 s before continuing to rise. This second increase in C_6H_6 intensity occurred before applying the heating ramp (at 16500 s), indicating that the surface was warm enough for C_6H_6 desorption to occur. The remaining C_6H_6 and C_2H_2 desorbed from the surface

when the dust temperature increased through the controlled removal of dry ice from the cooler box.

C_6H_6 can exist in more than a dozen isomeric forms which could give rise to the observed signal at m/z = 78. However, there are three pieces of evidence that the C_6H_6 species in the present study is benzene. First, Figure 7 shows a typical set of C_2H_2 and C_6H_6 TPD traces resulting from a C_2H_2 uptake experiment at 115 K. Also shown in this plot is a TPD trace of benzene directly dosed onto the olivine dust in a separate experiment. Note that both C_6H_6 desorption peaks have coincident falling edges (within experimental error), which is typical of sub-monolayer coverages desorbing from a surface containing multiple binding sites e.g. Thrower et al. (2009). It is unlikely that other C_6H_6 isomers would have such similar temperature-dependent desorption kinetics as benzene. Second, cyclo-trimerization studies of C_2H_2 at low temperatures on metal surfaces have identified benzene as the C_6H_6 product through ultraviolet photoelectron spectroscopy (Sesselmann et al., 1983; Tysoe et al., 1983) and high-resolution electron energy loss spectroscopy (Jungwirthova and Kesmodel, 2000). Third, consideration of the reaction energetics indicates that benzene is most likely the C_6H_6 product. All linear forms of C_6H_6 (e.g. 2,4-hexadiyne) and fulvene are very unlikely to form at low temperatures because at least one *sp* H atom shift would be required, involving a large energy barrier. For the remaining compounds where an H atom shift is not required, we have calculated the enthalpy of formation from 3 C_2H_2 molecules at the cbs-qb3 level of theory (Frisch et al., 2009). The $\Delta H^{\ominus}$ values are -597, -290, -271 and -117 kJ mol^{-1} for benzene, benvalene, dewar benzene and prismane, respectively. The enormous relative stability of benzene is consistent with the experimental evidence (see above) that this is the form of C_6H_6 produced in the present study.
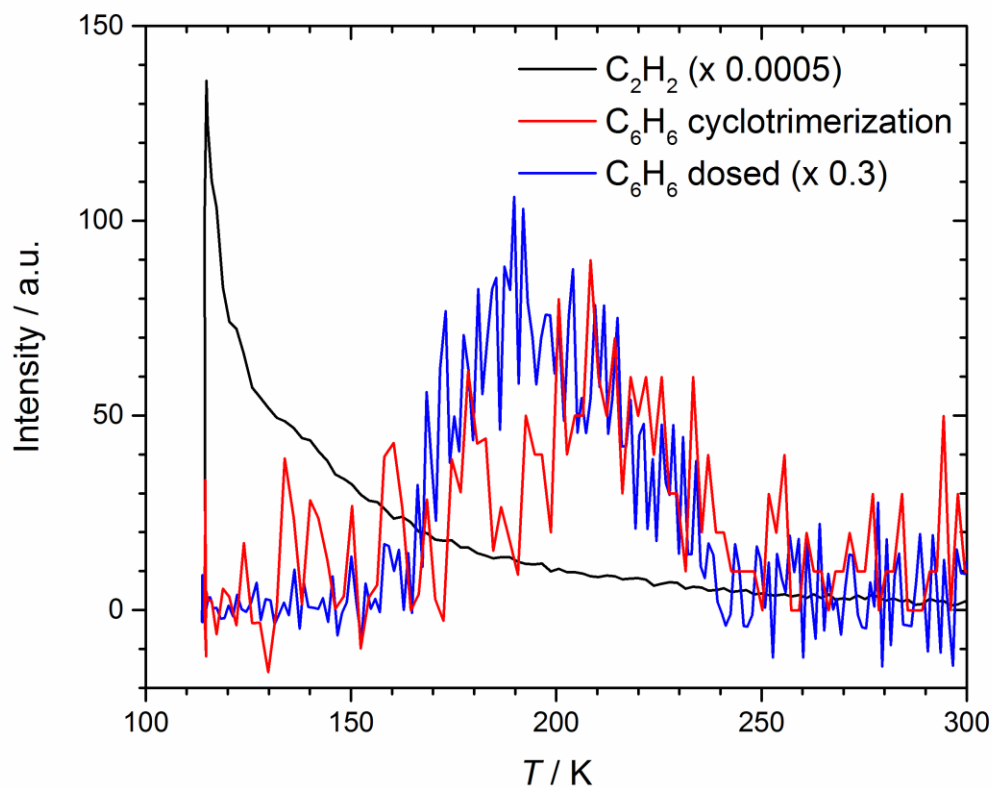
Figure 7. C_2H_2 and C_6H_6 TPD traces obtained from C_2H_2 cyclo-trimerization, and C_6H_6 dosed directly onto the Fe_2SiO_4 sample, which was held at 115 K.

The intermediate species C_4H_4 was also monitored during these experiments but the mass trace (not shown) remained below the QMS detection limit indicating that this species, if formed, is a short-lived intermediate which undergoes further reaction on the surface to form the observed C_6H_6. Hence, the steady-state concentration of C_4H_4 was too low to observe by TPD under our experimental conditions, as in studies of cyclo-trimerization on palladium crystal surfaces (Abbet et al., 2001; Janssens et al., 1998). In contrast, cyclo-trimerization studies of C_2H_2 on palladium and copper surfaces have detected C_4H_4 by using techniques which directly probe the surface e.g. near-edge X-ray absorption fine structure (Ormerod et

al., 1993b), laser-induced thermal desorption spectroscopy (Abdelrehim et al., 1995), temperature programmed reaction (Kyriakou et al., 2005), and sum frequency generation (Öberg et al., 2012).

In order to confirm that C_6H_6 was produced from C_2H_2 cyclo-trimerization, rather than being an impurity in the C_2H_2, a set of C_2H_2 dosed time delay TPD experiments were performed using the UHV apparatus. Here, C_2H_2 was dosed onto the Fe_2SiO_4 coated sample with the sample held at 130 K for 7940 s. The time between terminating the C_2H_2 dose and starting the TPD linear heating ramp was varied in order to examine whether the amount of C_6H_6 observed changed with respect to the delay time. The C_6H_6 TPD yield was obtained by integrating the C_6H_6 TPD peak with respect to time. Figure 8 demonstrates a clear linear trend between C_6H_6 TPD yield and the delay time, which passes through the origin (within experimental error). This confirms that the source of the C_6H_6 mass trace observed in this study was cyclo-trimerization of C_2H_2 on the dust analogue surface.
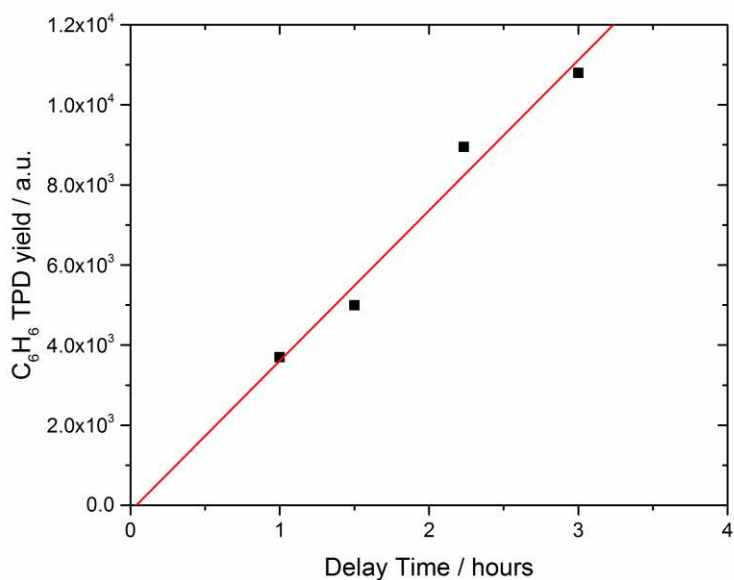
Figure 8. C_6H_6 TPD yield plotted as a function of the time delay between termination of the C_2H_2 dose (with the Fe_2SiO_4 sample held at 130 K) and start of the TPD linear heating ramp.

The first-order cyclo-trimerization rate of C_2H_2 to form ⅓ of a C_6H_6 molecule, k_{CT}, in the dual flow tube experiments was calculated by dividing the production rate of C_6H_6 molecules per second by C_2H_{2surf}, when the dust analogue becomes saturated with C_2H_2 (before the gas mixture was switched to pure He). On Mg_2SiO_4, a mean of four separate experiments gave k_{CT} = $(5.0 \pm 1.7) \times 10^{-7}$ s^{-1} with a 1 standard deviation error. A single experiment was performed on Fe_2SiO_4 giving k_{CT} = 1.7×10^{-7} s^{-1} which is probably within experimental error of the result on Mg_2SiO_4. For modelling purposes (Section 4), we use an overall value for k_{ct} on olivines of $(4.3 \pm 2.1) \times 10^{-7}$ s^{-1}.

The temperature dependence of k_{CT} was investigated using the UHV apparatus by dosing C_2H_2 onto the sample held at 115, 130 and 181 K for a fixed delay time (8040 s) before performing TPD analysis. A typical set of C_2H_2 and C_6H_6 traces are displayed in Figure 7. The desorption peak for C_2H_2 begins immediately indicating that C_2H_2 was desorbing from the Fe_2SiO_4 surface during the dose and subsequent delay time. The surface concentrations of C_2H_2 and C_6H_6 at each sample temperature were obtained from the corresponding TPD peak using the same procedure as that for the C_6H_6 TPD yield. The C_6H_6 surface concentration was divided by the delay time (i.e. the time between the end of the C_2H_2 dose and the start of the TPD) and the C_2H_2 surface concentration to give k_{CT}. The results at 115, 130 and 181 K are $(4.1 \pm 1.1) \times 10^{-8}$, $(2.5 \pm 0.6) \times 10^{-7}$ and $(2.0 \pm 0.5) \times 10^{-6}$ s^{-1}, respectively. Thus, k_{CT} increases with temperature, which has been seen previously in studies of C_2H_2 cyclo-trimerization on Pd (Abdelrehim et

al., 1996; Janssens et al., 1998). Note that the UHV value of k_{CT} at 181 K is larger by a factor of

~ 5 than the corresponding value obtained using the dual flow tube apparatus (at the same

temperature). This is because the TPD data does not account for the decrease in the C_2H_2

surface concentration due to desorption after the C_2H_2 dosing is stopped; hence the UHV

method provides an upper limit for k_{CT} at 181 K. However, at 115 K the desorption of C_2H_2

would be much slower, and hence the k_{CT} value measured at this temperature should be

correct. Combining this 115 K value with the 181 K measurement in the dual flow tube yields

the Arrhenius expression $k_{CT} = 2.6 \times 10^{-5} \exp(-741/T)$ s^{-1}. Taking account of the errors in the

two measured data points, the error in k_{CT} varies from ± 27 to $\pm 49\%$ between 115 and 181 K.

4. Implications for Titan's Atmosphere

4.1 Modelling the cosmic dust abundance

To explore the formation of C_6H_6 in Titan's atmosphere *via* the heterogeneous chemistry of

C_2H_2 on un-ablated cosmic dust particles, a 1D model was constructed. The vertical profiles

of temperature, eddy diffusion coefficient (K_{zz}), pressure and C_2H_2 number density and were

taken from the Caltech/JPL 1D model of Titan's atmosphere (Allen et al., 1981; Gladstone et

al., 1996; Li et al., 2014; Yung et al., 1984; Zhang et al., 2010), and interpolated onto a 1 km

resolution grid extending from 0 to 605 km. These profiles are illustrated in Figure 9.
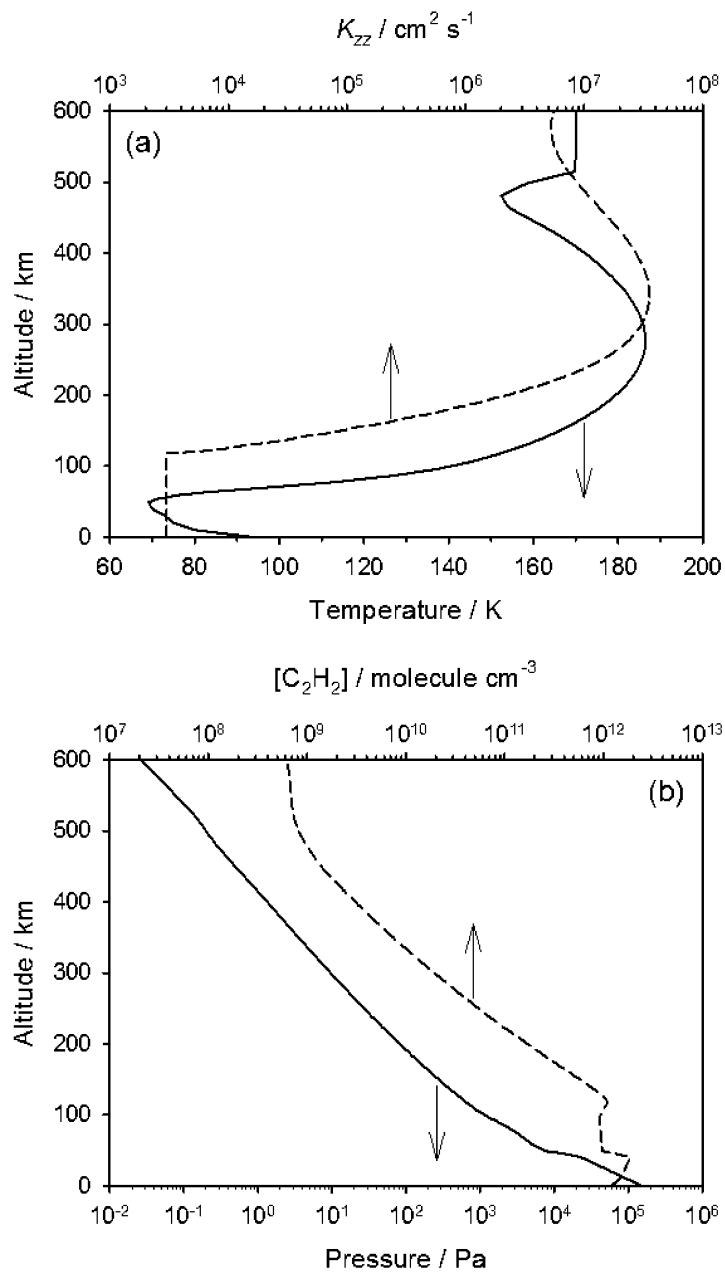
Figure 9. Vertical profiles of (a) temperature and eddy diffusion coefficient (K_{zz}) and (b) pressure and C_2H_2 concentration in Titan's atmosphere, taken from the Caltech/JPL 1D model (Li et al., 2014).

Data collected from the Pioneer 10 meteoroid detector and from the Student Dust Counter (SDC) on the New Horizons mission has been modelled by Poppe and Horanyi (2012) to obtain the differential number flux ($d\phi/dlog_{10}(r)$) of dust particles from the EKB entering the

Saturnian system, including Saturn's satellites and rings. In a recent update, Poppe (2016) has now added contributions from Jupiter Family (JFC), Halley Type (HTC), and Oort Cloud (OTC) comets into the model. Figure 10 illustrates the contributions from each of these sources, and the resulting total differential flux of particles into Titan's atmosphere. It should be noted that the Oort Cloud flux is really an upper limit, since the Pioneer 10 data can, strictly speaking, be fit with only contributions from JFC and EKB grains. While the HTC grains are included for completeness, they contribute very little to the overall flux. The modelled differential flux can be fit to the following parameterisation of particle radius r (in m):

$$\mathrm{d}\phi / \mathrm{dlog}_{10}(r) / \text{particle m}^{-2}\,\text{s}^{-1} = 6.22 \times 10^{-34} \times r^{-[7.96 + 0.506\,\log 10(r)]} \tag{6}$$

Figure 9 shows this parameterisation extrapolated from the particle size range measured (0.45 - 100 μm) down to 20 nm. The gradual fall-off in the differential flux is expected because solar radiation pressure ejects very small particles from the solar system (Nesvorný et al., 2010), and the Saturnian magnetosphere may also prevent small particles reaching the moons, as has been modelled in the case of Jupiter (Colwell and Horanyi, 1996). The dust is assumed to have a density of 2500 kg m^{-3} (Han et al., 2011), and was segregated into 38 size bins increasing geometrically in particle radius from 0.016 to 129 μm. The total mass of un-ablated cosmic dust into Titan's atmosphere is then 0.14 tonnes per earth day, which is an order of magnitude less a previous estimate of 1.4 t d^{-1} (Molina-Cuberos et al., 2001). However, this estimate was based on extrapolations of dust grain models from 1 AU, which Poppe (2016) has pointed out will over-predict the mass input by about 1 order. In any case, the differential flux illustrated in Figure 9 is essentially based on two data points (Pioneer 10 and the SDC), so is probably uncertain within an order of magnitude.
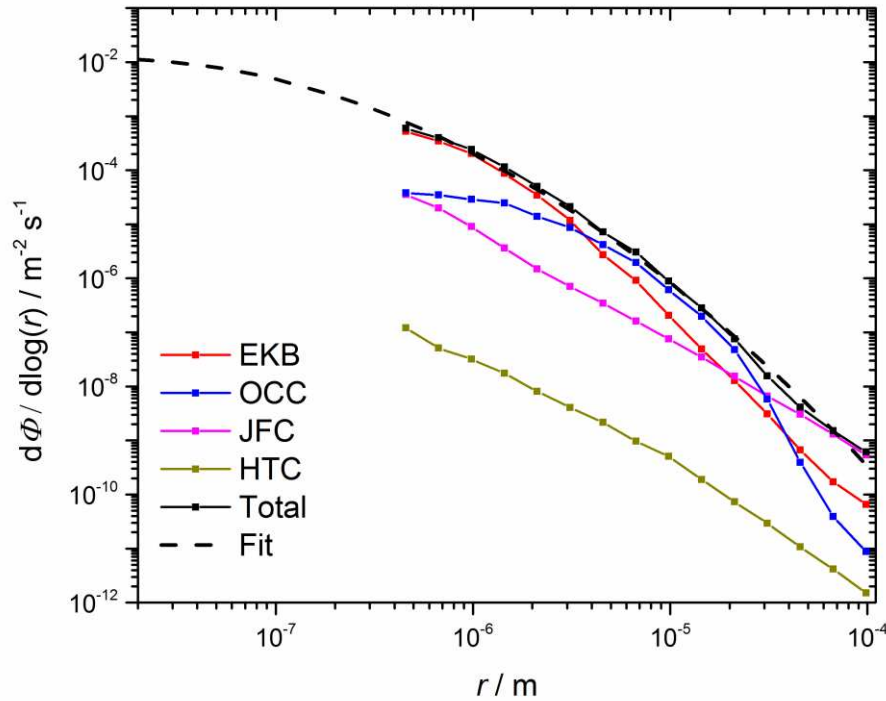
Figure 10. Differential flux of cosmic dust particles into Titan's atmosphere, showing the total flux made up of particles from the following sources: EKB=Edgeworth Kuiper Belt; JFC=Jupiter family comets; HTC=Halley comets; OCC=Oort Cloud comets. The line labelled Fit is the parameterisation in eqn. 6.

We now examine the fraction of these dust particles that will ablate. The Chemical ABlation MODel (CABMOD) (Vondrak et al., 2008) was adapted to treat meteoric ablation in Titan's atmosphere starting at 1200 km. For a given meteoroid mass, velocity and entry angle, CABMOD predicts the ablation rate of individual meteoric elements through sputtering (i.e. through inelastic collisions with atmospheric molecules), and by evaporation of oxides and atoms once the particle melts. EKB particles were taken to have an olivinic composition, as determined by the analysis of Comet 81P/Wild 2 dust samples (Gainsforth et al., 2015;

26

Zolensky et al., 2006), with an Fe:Mg ratio of ~0.6: this implies, according to the olivine phase diagram, the particles melting at 1750 K (Vondrak et al., 2008). Figure 11 is an example of CABMOD output, showing the predicted elemental injection rates for a meteoroid with an entry velocity of 18 km s^{-1} and a mass of 100 µg. The most volatile elements, Na and K, are released at ~550 km, whereas the main constituents Fe, Si and Mg are released about 70 km closer to the surface. Because of Titan's large scale height, which is roughly 40 km at these meteoric ablation altitudes, ablation occurs over a much wider range of altitudes compared to the terrestrial planets (Molina-Cuberos et al., 2008; Vondrak et al., 2008; Whalley and Plane, 2010).
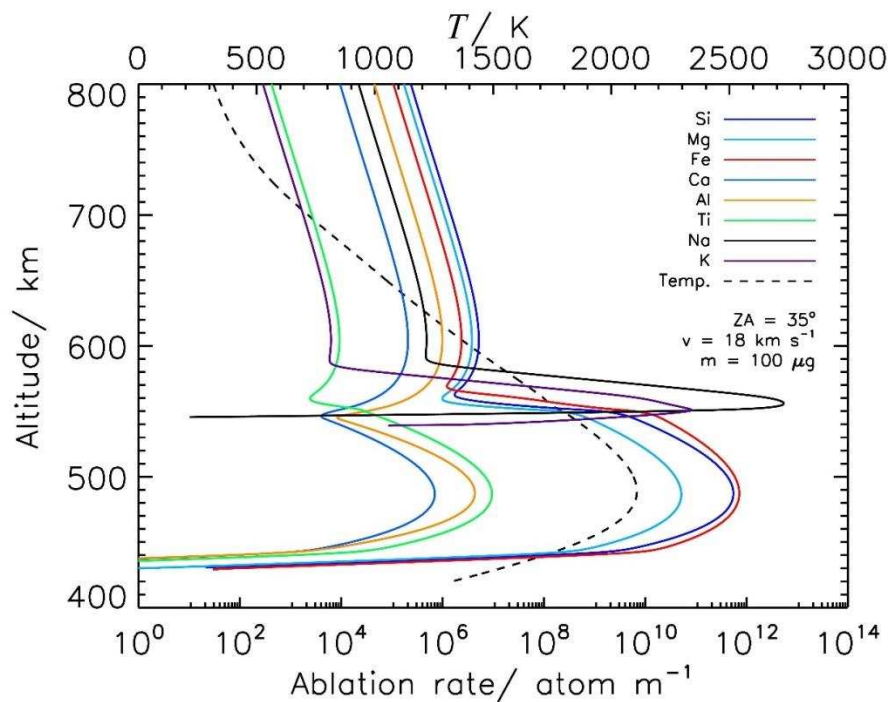
Figure 11. Ablation profiles of individual elements for a 100 µg (r = 200 µm) meteoroid entering Titan's atmosphere at 18 km s-1 and 35° to zenith.

Figure 12 shows the mass fraction of a meteoroid that ablates, plotted as a function of particle radius/mass and entry velocity. The dust entry velocity into Titan's atmosphere ranges from

2.6 - 29.1 km s^{-1}, with a mean of 18 km s^{-1} (Molina-Cuberos et al., 2001). The plot shows that particles smaller than 10 μm do not reach the melting point of 1750 K, so a very small fraction (<1%) of mass is lost by sputtering. Larger particles exhibit more severe loss through melting and evaporation, so a particle of 200 μm (~100 μg) loses up to 90% of its mass at the highest entry velocities. However, these larger particles sediment very rapidly through Titan's atmosphere; it is only particles smaller than 10 μm that contribute significantly to the available surface area for heterogeneous chemistry (see below).
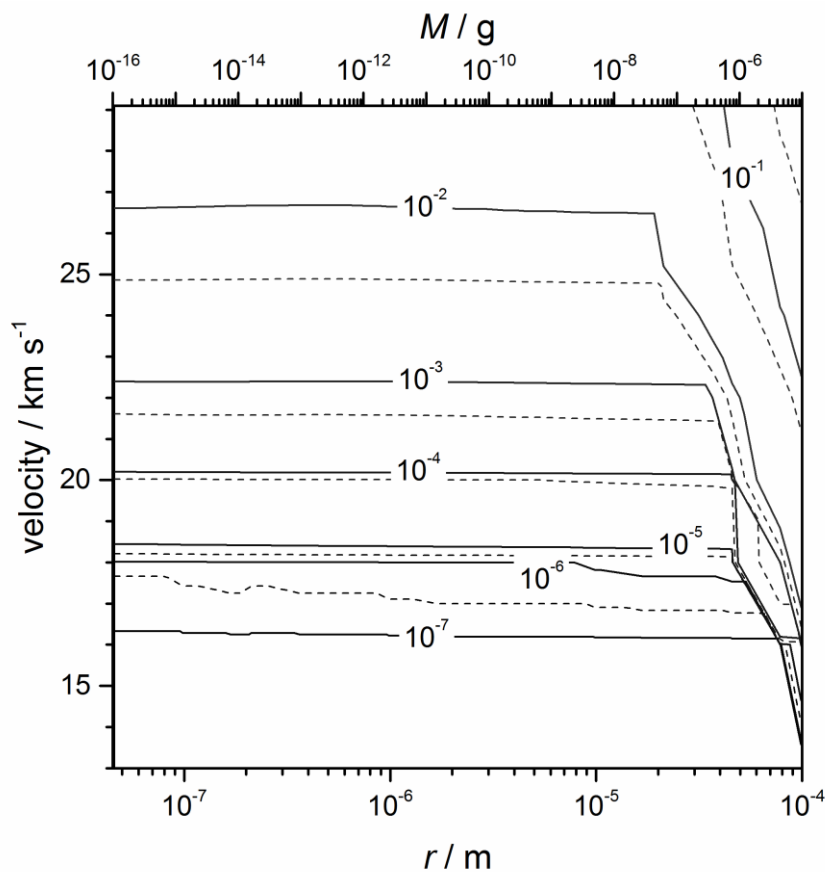
Figure 12. Ablated fraction of a meteoroid with a particle density of 2500 kg m^{-3} as a function of mass and velocity.

The flux of dust particles of different sizes being transported vertically by eddy diffusion and sedimentation is given by:

$$\phi_i = -K_{zz}\left\{\frac{\partial N_i}{\partial z} + \left(\frac{1}{T}\frac{\partial T}{\partial z} + \frac{1}{H}\right)N_i\right\} + w_i N_i \qquad (7)$$

where ϕ_i is the vertical flux of particles in dust size bin i, K_{zz} is the eddy diffusion coefficient, N_i is the dust number density, H is the atmospheric scale height, and w_i is the sedimentation velocity. w_i can be determined from a form of Stokes' law which describes a spherical particle falling through a stationary fluid (Jacobson, 2005):

$$w_i = \frac{2(\rho_{dust} - \rho_{air})}{9\mu} g\, r_i{}^2 C_{scf} \qquad (8)$$

where ρ_{dust} and ρ_{air} are the dust and air density; μ is the dynamic viscosity of N_2 at temperature T; g is the gravitational constant (1.352 m s^{-2} for Titan); r_i is the particle radius and C_{scf} is the Cunningham slip correction factor which takes into account the non-continuum effects of drag on small particles. C_{scf} is estimated from equation 9, where λ is the mean free path of the air molecules, and A_1, A_2 and A_3 are dimensionless coefficients which for N_2 are equal to 1.249, 0.42 and 0.87, respectively (Kasten, 1968).

$$C_{scf} = 1 + \frac{\lambda}{r_i}\left(A_1 + A_2 exp\left(\frac{-A_3 r_i}{\lambda}\right)\right) \qquad (9)$$

Because the number density of these un-ablated cosmic dust particles is relatively small, and they rapidly become coated with a monolayer of C_2H_2 (see below), coagulation should not play a major role as they descend through the atmosphere. Under steady-state conditions, the flux of particles in each size bin is then constant throughout the atmosphere to the surface. Equation 7 was solved using a time-implicit integration scheme (Shimazaki, 1985). Figure 13 shows the resulting size distributions of particle number density (N) and volumetric

surface area (A_s), as a function of height between the surface and 600 km. It is clear that most of the available surface area for heterogeneous chemistry is below 150 km, and is provided by small particles (0.04 < r < 2 µm). The highest values of A_s are therefore located in the same atmospheric region as the main haze layer below ~ 220 km (Rages and Pollack, 1983; Smith et al., 1981).
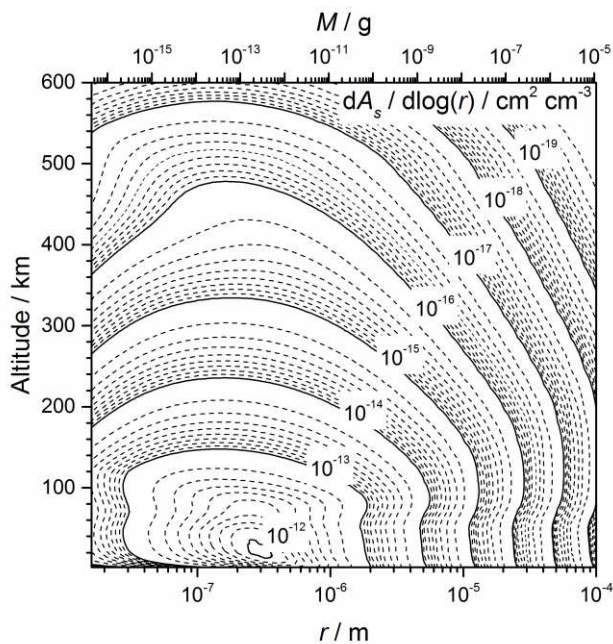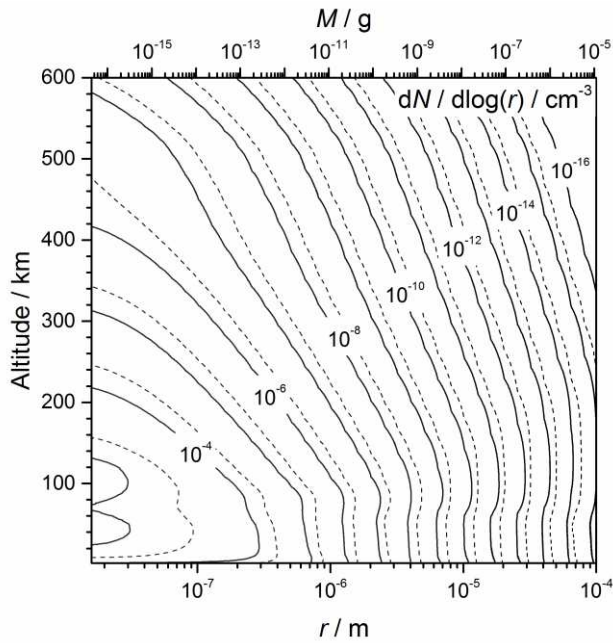
Figure 13. A plot of the size distribution of un-ablated cosmic dust particle number density, *N*, (top panel) and volumetric surface area, *As*, (bottom panel) as a function of altitude.

4.2 Heterogeneous chemical kinetics

The kinetics of C_2H_2 uptake, cyclo-trimerization and C_6H_6 desorption were then treated by solving the following coupled differential equations for the time that the particles spend in each model layer during their descent to the surface:

$$\frac{d[C_2H_2{}^{ads}]}{dt} = \frac{\gamma}{4}\bar{c}A_s[C_2H_2] - k_{CT}[C_2H_2{}^{ads}] \tag{11}$$

$$\frac{d[C_6H_6{}^{ads}]}{dt} = \frac{k_{CT}[C_2H_2{}^{ads}]}{3} - k_d[C_6H_6{}^{ads}] \tag{12}$$

$$\frac{d[C_6H_6]}{dt} = k_d[C_6H_6{}^{ads}] \tag{13}$$

where k_d is the first-order rate of C_6H_6 desorption. Since the composition of the EKB dust particles is assumed to be chondritic (Gainsforth et al., 2015; Zolensky et al., 2006) and hence essentially olivinic, we use here the mean measured value for γ of 1.7×10^{-4}. Note that the laboratory measurement was made at 181 K, and the temperature dependence of γ could not be measured at lower temperatures using the flow tube system. Since uptake coefficients typically have negative temperature dependences (see discussion in Frankland et al. (2015)), γ is probably higher in most of Titan's atmosphere below 300 km (Flasar et al., 2005), and so the rate of uptake should be a lower limit.

The uptake of C_2H_2 was restricted to sub-monolayer coverage (i.e. < 10^{15} molecule cm^{-2}). This was achieved in the model by ensuring that as the coverage of C_2H_2 and C_6H_6 approached this limit, γ in eqn. 11 was reduced to zero in proportion to the remaining available adsorption sites on the dust particle. Note that although the adsorption of other less volatile species in Titan's atmosphere could reduce the available surface sites for C_2H_2 adsorption, C_2H_2 is the second most abundant minor species in Titan's atmosphere with a mixing ratio which remains fairly constant between 500 and 150 km (Teanby et al., 2006), as shown in Figure 9b. Furthermore, Titan's atmospheric temperature is too high for the most abundant species in Titan's atmosphere (N_2 and CH_4) to be physisorbed on the cosmic dust surface (Chickos and Acree, 2002; Collings et al., 2015).

The temperature-dependent C_2H_2 cyclo-trimerization rate on olivine measured in this study is k_{CT} = 2.6 × 10^{-5} exp(-741/T) s^{-1}. The rate of desorption of C_6H_6 was set equal to k_d = 9 × 10^{12} exp(-45 kJ mol^{-1} / RT) s^{-1}, where first-order desorption kinetics are assumed because the coverage of C_6H_6 on the dust surface will be sub-monolayer, as cyclo-trimerisation only occurs on surface-active sites. The pre-exponential factor is set to the vibrational frequency of a C_6H_6 molecule against the olivine surface. We have calculated this using electronic structure theory at the B3LYP/6-311+g(2d,p) level in the Gaussian G09 program (Frisch et al., 2009). Figure 14 illustrates a C_6H_6 molecule bound to a surface Fe atom. The arrows on the atoms are displacement vectors of the vibrational mode corresponding to desorption, which has a calculated frequency of 302 cm^{-1} (=9 × 10^{12} s^{-1}), a typical value for desorption kinetics (Attard and Barnes, 1998). The binding energy in the exponential term was set to 45 kJ mol^{-1}, which has been measured for the sublimation of C_6H_6 (Chickos and Acree, 2002).
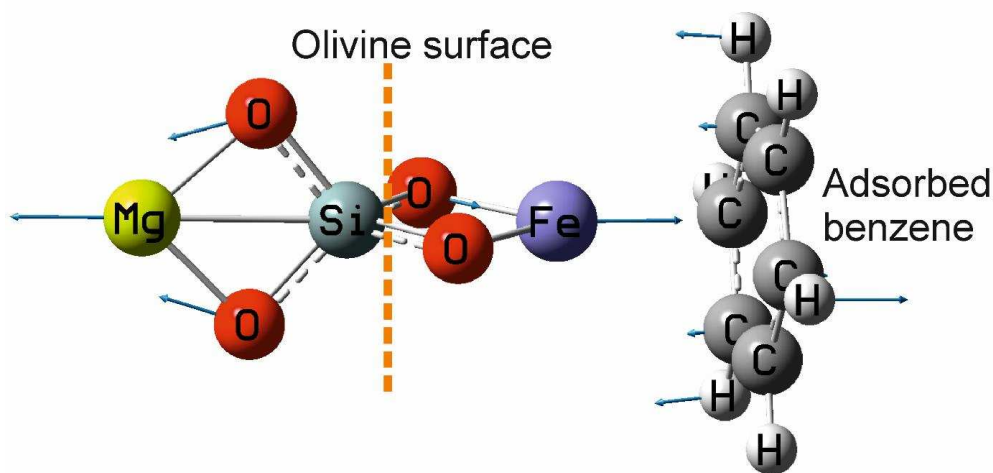
Figure 14. A C_6H_6 molecule adsorbed onto an Fe atom at the olivine surface (at the B3LYP/6-311+g(2d,p) level of theory). The blue arrows on the atoms are displacement vectors for the vibration at 302 cm^{-1}, which is an Fe-C_6H_6 stretch orthogonal to the surface corresponding to the desorption coordinate.

4.3 Production of C_6H_6

Figure 15 shows the modelled rate of C_6H_6 production between 600 km and the surface, resulting from C_2H_2 uptake, cyclo-trimerization, and desorption of C_6H_6. The production rate increases by a factor of 10^7 between 600 and 90 km. There are two reasons for this: the dust surface area increases by a factor of ~10^5 because the sedimentation rate of the particles decreases with decreasing height; and the C_2H_2 number density increases by a factor of ~1500 (Figure 9b). Above 80 km, the ratio of adsorbed C_2H_2 to C_6H_6 on the dust is > 10^4, consistent with C_6H_6 desorption not being rate-limiting. Model sensitivity experiments show that the cyclo-trimerization step is rate-determining above 80 km, so the *kinetic* uncertainty in the C_6H_6 production rate between 80 and 550 km arises from the ~$\pm$50% uncertainty in k_{CT} (Section 3); in contrast, decreasing k_d by a factor of 10 has a negligible effect on the C_6H_6 production rate profile. The greatest contribution to the uncertainty in the C_6H_6 production

rate arises from the order-of-magnitude uncertainty in the dust flux into Titan's atmosphere (Poppe, 2016), and this is illustrated by the uncertainty envelope in Figure 15.
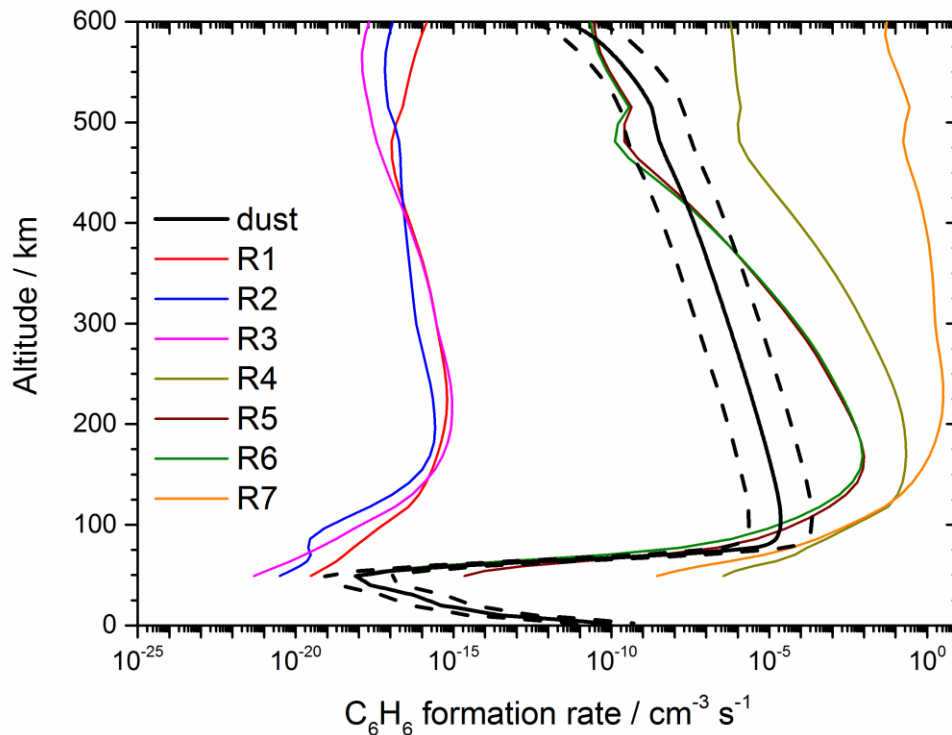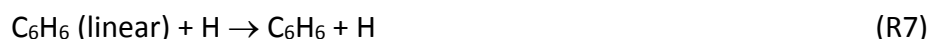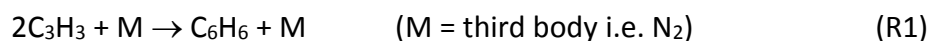

Figure 15. The C_6H_6 production rate from the uptake of C_2H_2 on cosmic dust, cyclo-trimerization and desorption, shown as a function of altitude. The dashed lines encapsulate the uncertainty in the dust flux into Titan's atmosphere. The heterogeneous rate is also compared to gas-phase C_6H_6 formation rates (reaction numbers defined in the text).

Below 90 km the C_6H_6 production rate mirrors the temperature profile (Figure 9a): the temperature falls rapidly from 130 K at 90 km to 70 K at 50 km, before warming up to 94 K near the surface (Yung et al., 1984). Because k_d has a significant activation energy (see above), at these cold temperature desorption of C_6H_6 becomes very slow and rate-limiting, so that

the dust particles smaller than 0.2 μm become completely coated in C_6H_6 and further uptake of C_2H_2 ceases. At this point there is the possibility that photochemistry (or possibly cosmic-ray induced chemistry) could lead to the formation of larger organic molecules such as polyaromatic hydrocarbons (PAHs) on the dust surface.

The heterogeneous C_6H_6 formation rate can be compared with direct gas-phase production (Wilson et al., 2003), which occurs *via* the following seven reactions in the Caltech/JPL model (Allen et al., 1981; Gladstone et al., 1996; Li et al., 2014; Yung et al., 1984; Zhang et al., 2010):

$$2C_3H_3 + M \rightarrow C_6H_6 + M \qquad (M = \text{third body i.e. } N_2) \qquad \text{(R1)}$$

$$H + C_6H_5 + M \rightarrow C_6H_6 + M \qquad \text{(R2)}$$

$$CH_3 + C_5H_3 + M \rightarrow C_6H_6 + M \qquad \text{(R3)}$$

$$C_4H_5 + C_2H_2 \rightarrow C_6H_6 + H \qquad \text{(R4)}$$

$$C_6H_5 + H_2 \rightarrow C_6H_6 + H \qquad \text{(R5)}$$

$$C_6H_5 + CH_4 \rightarrow C_6H_6 + CH_3 \qquad \text{(R6)}$$

$$C_6H_6 \text{ (linear)} + H \rightarrow C_6H_6 + H \qquad \text{(R7)}$$

The rates of these C_6H_6 formation routes calculated in the JPL model are also depicted in Figure 15, which shows that heterogeneous production may well be competitive with reactions 4 - 7 between 80 and 120 km. In fact, recent experimental work at the University of Leeds has shown that a key photochemical intermediate in this gas-phase chemistry, singlet methylene ($^1CH_2$), is quenched by N_2 much more rapidly to the relatively unreactive $^3CH_2$ ground state at temperatures below 150 K than extrapolations from above 250 K indicate (pers. comm. K. Douglas). This will reduce the efficiency of these gas-phase production routes and increase the relative importance of heterogeneous production.

A final point concerns the deposition of C_6H_6 to the surface. In the very cold lower troposphere the cosmic dust particles are likely to be coated with C_6H_6 (see above); the direct deposition of coated particles to the surface would then constitute a flux of about 3 molecule cm^{-2} s^{-1}. The downward flux of gas-phase C_6H_6 can be estimated using equation 7 (with the dust sedimentation velocity w = 0) and the modelled mixing ratio gradient at 50 km (5.2 ppt km^{-1}), yielding ~1 × 10^6 molecule cm^{-2} s^{-1}. Even allowing for uncertainties in K_{zz} and the dust flux, deposition from the gas phase should clearly dominate.

5. Summary and Conclusions

This study shows that the uptake of C_2H_2 on cosmic dust particles may be a significant source of C_6H_6 in Titan's atmosphere. Because of the relatively small mass of the moon, dust particles enter at low speeds and encounter an atmosphere where the pressure increases gradually. Hence a much smaller fraction of the particles ablate compared with the terrestrial planets, providing a significant surface area for heterogeneous chemistry. The uptake coefficient of

C_2H_2 on olivine particles (synthesized as analogues of cosmic dust), and the temperature-dependent rate of cyclo-trimerization to form C_6H_6 were measured in a flow tube and a UHV apparatus. The uptake coefficient on a range of olivine compositions from forsterite to fayalite was $(1.7 \pm 0.4) \times 10^{-4}$. The first-order cyclo-trimerization rate was $2.6 \times 10^{-5} \exp(-741/T)$ s^{-1} between 115 and 181 K, and was also independent of Mg/Fe ratio in the olivine.

The chemical ablation model CABMOD was used to show that for dust particles between 0.02 and 10 μm in radius entering Titan's atmosphere at speeds up to the maximum of 29 km s^{-1}, less than 1% of mass loss occurred through sputtering. Significant mass loss did not occur because the particle temperature did not reach 1750 K when melting and evaporation would cause much more rapid ablation. A 1D model describing the sedimentation of cosmic dust between 600 km and the surface of Titan, together with C_2H_2 uptake, cyclo-trimerization and desorption of C_2H_6, shows that this heterogeneous pathway is probably competitive with the gas-phase production routes included in existing models between 80 and 120 km in Titan's troposphere.

6. Acknowledgements

References:

Abbet, S., Sanchez, A., Heiz, U., Schneider, W. D., 2001. Tuning the selectivity of acetylene polymerization atom by atom. J. Catalysis. 198**,** 122-127.

Abdelrehim, I. M., Caldwell, T. E., Land, D. P., 1996. Coverage effects on the kinetics of benzene formation from acetylene on Pd(111): A laser-induced thermal desorption Fourier transform mass spectrometry investigation. J. Phys. Chem. 100**,** 10265-10268.

Abdelrehim, I. M., Thornburg, N. A., Sloan, J. T., Caldwell, T. E., Land, D. P., 1995. Kinetics and Mechanism of Benzene Formation from Acetylene on Pd(111) Studied by Laser-Induced Thermal-Desorption Fourier-Transform Mass-Spectrometry. Journal of the American Chemical Society. 117**,** 9509-9514.

Allen, M., Yung, Y. L., Waters, J. W., 1981. Vertical transport and photochemistry in the Terrestrial mesosphere and lower thermosphere (50-120 km). J. Geophys. Res. 86**,** 3617.

Attard, G., Barnes, C., 1998. Surfaces. Oxford University Press, Oxford.

Brunauer, S., Emmett, P. H., Teller, E., 1938. Adsorption of gases in multimolecular layers. J. Am. Chem. Soc. 60**,** 309-319.

Cable, M. L., Horst, S. M., Hodyss, R., Beauchamp, P. M., Smith, M. A., Willis, P. A., 2012. Titan Tholins: Simulating Titan Organic Chemistry in the Cassini-Huygens Era. Chem. Rev. 112**,** 1882-1909.

Chickos, J. S., Acree, W. E., 2002. Enthalpies of sublimation of organic and organometallic compounds. 1910-2001. J. Phys. Chem. Ref. Data. 31**,** 537-698.

Coll, P., et al., 2013. Can laboratory tholins mimic the chemistry producing Titan's aerosols? A review in light of ACP experimental results. Planet. Space Sci. 77**,** 91-103.

Collings, M. P., Frankland, V. L., Lasne, J., Marchione, D., Rosu-Finsen, A., McCoustra, M. R. S., 2015. Probing model interstellar grain surfaces with small molecules. Mon. Not. Roy. Astron. Soc. 449**,** 1826-1833.

Colwell, J. E., Horanyi, M., 1996. Magnetospheric effects on micrometeoroid fluxes. Geophys. Res. Lett. 101**,** 2169-2175.

Coustenis, A., et al., 2010. Titan trace gaseous composition from CIRS at the end of the Cassini-Huygens prime mission. Icarus. 207**,** 461-476.

Dobrijevic, M., Hebrard, E., Loison, J. C., Hickson, K. M., 2014. Coupling of oxygen, nitrogen, and hydrocarbon species in the photochemistry of Titan's atmosphere. Icarus. 228**,** 324-346.

English, M. A., Lara, L. M., Lorenz, R. D., Ratcliff, P. R., Rodrigo, R., 1996. Ablation and chemistry of meteoric materials in the atmosphere of Titan. Adv. Space Res. 17**,** 157-160.

Flasar, F. M., et al., 2005. Titan's atmospheric temperatures, winds, and composition. Science. 308**,** 975-978.

Frankland, V. L., Alexander, J. D., Feng, W., Plane, J., 2015. The uptake of HNO_3 on meteoric smoke analogues. J. Atmos. Solar-Terr. Phys. 127**,** 150-160.

Frisch, M. J., et al., 2009. Gaussian 09, Revision A.1. Gaussian, Inc., Wallingford CT.

Gainsforth, Z., et al., 2015. Constraints on the formation environment of two chondrule-like igneous particles from comet 81P/Wild 2. Meteor. Planet. Sci. 50**,** 976-1004.

Gladstone, G. R., Allen, M., Yung, Y. L., 1996. Hydrocarbon photochemistry in the upper atmosphere of Jupiter. Icarus. 119**,** 1-52.

Han, D., Poppe, A. R., Piquette, M., Grun, E., Horanyi, M., 2011. Constraints on dust production in the Edgeworth-Kuiper Belt from Pioneer 10 and New Horizons measurements. Geophys. Res. Lett. 38.

Hebrard, E., Dobrijevic, M., Benilan, Y., Raulin, F., 2007. Photochemical kinetics uncertainties in modeling Titan's atmosphere: First consequences. Planet. Space Sci. 55**,** 1470-1489.

Hebrard, E., Dobrijevic, M., Loison, J. C., Bergeat, A., Hickson, K. M., Caralp, F., 2013. Photochemistry of C_3Hp hydrocarbons in Titan's stratosphere revisited. Astron. Astrophys. 552.

Hoffmann, H., et al., 1992. A near-Edge X-Ray Absorption Fine-Structure and Photoelectron Spectroscopic Study of the Structure of Acetylene on Pd(111) at Low-Temperature. Surface Sci. 268**,** 1-10.

Ip, W. H., 1990. Meteoroid Ablation Processes in Titans Atmosphere. Nature. 345**,** 511-512.

Jacobson, M. Z., 2005. Fundamentals of Atmospheric Modeling, 2nd edn.
Cambridge Univ. Press, New York.

Janssens, T. V. W., Volkening, S., Zambelli, T., Wintterlin, J., 1998. Direct observation of surface reactions of acetylene on Pd(111) with scanning tunneling microscopy. J. Phys. Chem. B. 102**,** 6521-6528.

Jungwirthova, I., Kesmodel, L. L., 2000. Benzene formation from acetylene on Pd(111): a high-resolution electron energy loss spectroscopy study. Surface Sci. 470**,** L39-L44.

Kasten, F., 1968. Falling speed of aerosol particles. J. App. Meteor. 7**,** 944-947.

Kelley, M. S., et al., 2013. The persistent activity of Jupiter-family comets at 3-7 AU. Icarus. 225**,** 475-494.

Krasnopolsky, V. A., 2010. The photochemical model of Titan's atmosphere and ionosphere: A version without hydrodynamic escape. Planet. Space Sci. 58, 1507-1515.

Krasnopolsky, V. A., 2012. Titan's photochemical model: Further update, oxygen species, and comparison with Triton and Pluto. Planet. Space Sci. 73, 318-326.

Krasnopolsky, V. A., 2014. Chemical composition of Titan's atmosphere and ionosphere: Observations and the photochemical model. Icarus. 236, 83-91.

Kyriakou, G., Kim, J., Tikhov, M. S., Macleod, N., Lambert, R. M., 2005. Acetylene Coupling on Cu(111): Formation of Butadiene, Benzene, and Cyclooctatetraene. J. Phys. Chem. B. 109, 10952–10956.

Landgraf, M., Liou, J. C., Zook, H. A., Grun, E., 2002. Origins of solar system dust beyond Jupiter. Astron. J. 123, 2857-2861.

Lara, L. M., Lellouch, E., Gonzalez, M., Moreno, R., Rengel, M., 2014. A time-dependent photochemical model for Titan's atmosphere and the origin of H_2O. Astron. Astrophys. 566.

Lavvas, P. P., Coustenis, A., Vardavas, I. M., 2008a. Coupling photochemistry with haze formation in Titan's atmosphere, part I: Model description. Planet. Space Sci. 56, 27-66.

Lavvas, P. P., Coustenis, A., Vardavas, I. M., 2008b. Coupling photochemistry with haze formation in Titan's atmosphere, Part II: Results and validation with Cassini/Huygens data. Planet. Space Sci. 56, 67-99.

Li, C., Zhang, X., Kammer, J. A., Liang, M.-C., Shia, R.-L., Yung, Y. L., 2014. A non-monotonic eddy diffusivity profile of Titan's atmosphere revealed by Cassini observations. Planet. Space Sci. 104, 48-58.

Liang, M.-C., Yung, Y. L., Shemansky, D. E., 2007. Photolytically generated aerosols in the mesosphere and thermosphere of Titan. Astrophys. J. 661, L199-L202.

Magee, B. A., Waite, J. H., Mandt, K. E., Westlake, J., Bell, J., Gell, D. A., 2009. INMS-derived composition of Titan's upper atmosphere: Analysis methods and model comparison. Planet. Space Sci. 57, 1895-1916.

Mangan, T. P., Frankland, V. L., Plane, J., 2015. CO_2 trapping in amorphous H_2O ice: relevance to polar mesospheric cloud particles. J. Atmos. Solar-Terr. Phys. 127, 92-96.

Molina-Cuberos, J. G., et al., 2001. Ionospheric layer induced by meteoric ionization in Titan's atmosphere. Planet. Space Sci. 49, 143-153.

Molina-Cuberos, J. G., Lopez-Moreno, J. J., Arnold, F., 2008. Meteoric layers in planetary atmospheres. Space Sci. Rev. 137, 175-191.

Nesvorný, D., Jenniskens, P., Levison, H. F., Bottke, W. F., Vokrouhlický, D., Gounelle, M., 2010. Cometary origin of the zodiacal cloud and carbonaceous micrometeorites. Implications for hot debris disks. Astrophys. J. 713, **816**-836.

Oakes, D. J., 1994. Dissociative adsorption of simple alkanes induced by hypertherman collisions with platinum. School of Chemical Sciences, Vol. PhD thesis. University of East Anglia.

Öberg, H., et al., 2012. Adsorption and Cyclotrimerization Kinetics of C2H2 at a Cu(110) Surface. J. Phys. Chem. C. 116, **9550**–9560.

Ormerod, R. M., Baddeley, C. J., Lambert, R. M., 1991. Geometrical and Electronic Effects in the Conversion of Acetylene to Benzene on Au(111)/Pd and Au/Pd Surface Alloys. Surface Sci. 259, **L709**-L713.

Ormerod, R. M., et al., 1993a. NEXAFS Identification of a Catalytic Reaction Intermediate - C_4H_4 on Pd(111). Surface Sci. 295, **277**-286.

Ormerod, R. M., et al., 1993b. NEXAFS identification of a catalytic reaction intermediate: C_4H_4 on Pd(111). Surface Science. 295, **277**-286.

Pacchioni, G., Lambert, R. M., 1994. Cyclization of Acetylene over Pd(111) - a Theoretical-Study of Reaction-Mechanisms and Surface Intermediates. Surface Sci. 304, **208**-222.

Patterson, C. H., Lambert, R. M., 1988. Molecular Mechanisms in the Cyclotrimerization of Acetylene to Benzene on Palladium(111). J. Phys. Chem. 92, **1266**-1270.

Patterson, C. H., Mundenar, J. M., Timbrell, P. Y., Gellman, A. J., Lambert, R. M., 1989. Molecular Pathways in the Cyclotrimerization of Acetylene on Pd(111) - Vibrational-Spectra of the C_4H_4 Intermediate and Its Thermal-Decomposition Products. Surface Sci. 208, **93**-112.

Plane, J. M. C., Feng, W., Dawkins, E. C. M., 2015. The Mesosphere and Metals: Chemistry and Changes. Chem. Rev. 115, **4497** - 4541.

Poppe, A. R., 2016. An improved model for interplanetary dust fluxes in the outer Solar System. Icarus. 264, **369**-386.

Poppe, A. R., Horanyi, M., 2012. On the Edgeworth-Kuiper Belt dust flux to Saturn. Geophys. Res. Lett. 39, **art**. no.: L15104.

Porco, C. C., et al., 2005. Imaging of Titan from the Cassini spacecraft. Nature. 434, **159**-168.

Rages, K., Pollack, J. B., 1983. Vertical-Distribution of Scattering Hazes in Titan Upper-Atmosphere. Icarus. 55, **50**-62.

Ramirez-Cuesta, A., Zgrablich, G., Tysoe, W. T., 1995. Simulation of Benzene Formation from Acetylene on Palladium and Oxygen-Covered Palladium Surfaces. Surface Sci. 340, **109**-118.

Saunders, R. W., Plane, J. M. C., 2011. A photo-chemical method for the production of olivine nanoparticles as cosmic dust analogues. Icarus. 212**,** 373-382.

Sekanina, Z., 1996. Activity of Comet Hale-Bopp (1995 O1) beyond 6 AU from the Sun. Astron. Astrophys. 314 957-965.

Sesselmann, W., Woratschek, B., Ertl, G., Kuppers, J., Haberland, H., 1983. Low-Temperature Formation of Benzene from Acetylene on a Pd(111) Surface. Surface Science. 130**,** 245-258.

Shemansky, D. E., Stewart, A. I. F., West, R. A., Esposito, L. W., Hallett, J. T., Liu, X. M., 2005. The Cassini UVIS stellar probe of the Titan atmosphere. Science. 308**,** 978-982.

Shimazaki, T., 1985. Minor Constituents in the Middle Atmosphere. D. Reidel Publishing Company, Dordrecht.

Smith, B. A., et al., 1981. Encounter with Saturn - Voyager-1 Imaging Science Results. Science. 212**,** 163-191.

Stern, S. A., 1996. Signatures of collisions in the Kuiper Disk. Astron. Astrophys. 310**,** 999-1010.

Teanby, N. A., et al., 2006. Latitudinal variations of HCN, HC_3N, and C_2N_2 in Titan's stratosphere derived from Cassini CIRS data. Icarus. 181**,** 243-255.

Thrower, J. D., Collings, M. P., Rutten, F. J. M., McCoustra, M. R. S., 2009. Laboratory investigations of the interaction between benzene and bare silicate grain surfaces. Mon. Not. Roy. Astron. Soc. 394**,** 1510-1518.

Tysoe, W. T., Nyberg, G. L., Lambert, R. M., 1983. Photoelectron-Spectroscopy and Heterogeneous Catalysis - Benzene and Ethylene from Acetylene on Palladium (111). Surface Science. 135**,** 128-146.

Vinatier, S., et al., 2010. Analysis of Cassini/CIRS limb spectra of Titan acquired during the nominal mission I. Hydrocarbons, nitriles and CO_2 vertical mixing ratio profiles. Icarus. 205**,** 559-570.

Vondrak, T., Plane, J. M. C., Broadley, S., Janches, D., 2008. A chemical model of meteoric ablation. Atmos. Chem. Phys. 8**,** 7015-7031.

Vondrak, T., Plane, J. M. C., Meech, S. R., 2006. Influence of submonolayer sodium adsorption on the photoemission of the Cu(111)/water ice surface. J. Chem. Phys. 125**,** art. no.: 224702.

Waite, J. H., et al., 2005. Ion Neutral Mass Spectrometer results from the first flyby of Titan. Science. 308**,** 982-986.

Whalley, C. L., Plane, J. M. C., 2010. Meteoric ion layers in the Martian atmosphere. Faraday Discuss. 147**,** 349-368.

Wilson, E. H., Atreya, S. K., 2003. Chemical sources of haze formation in Titan's atmosphere. Planet. Space Sci. 51**,** 1017-1033.

Wilson, E. H., Atreya, S. K., 2004. Current state of modeling the photochemistry of Titan's mutually dependent atmosphere and ionosphere. J. Geophys. Res. 109.

Wilson, E. H., Atreya, S. K., Coustenis, A., 2003. Mechanisms for the formation of benzene in the atmosphere of Titan. J. Geophys. Res. 108.

Yamamoto, S., Mukai, T., 1998. Dust production by impacts of interstellar dust on Edgeworth-Kuiper Belt objects. Astron. Astrophys. 329**,** 785-791.

Yung, Y. L., Allen, M., Pinto, J. P., 1984. Photochemistry of the atmosphere of Titan: comparison between model and observations. Astrophy. J. Suppl. Ser. 55**,** 465-506.

Zhang, X., Ajello, J. M., Yung, Y. L., 2010. Atomic Carbon in the Upper Atmosphere of Titan. Astrophys. J. Lett. 708**,** L18-L21.

Zolensky, M. E., et al., 2006. Report - Mineralogy and petrology of comet 81P/Wild 2 nucleus samples. Science. 314**,** 1735-1739.